Journal of Computational Physics **153,** 575–595 (1999)
Article ID jcph.1999.6296, available online at http://www.idealibrary.com on IDEAL®

On the Use of Nonlinear Filtering, Artificial Viscosity, and Artificial Heat Transfer for Strong Shock Computations

Song-Hyo Bae and Richard T. Lahey, Jr.

Center for Multiphase Research, Rensselaer Polytechnic Institute, Troy, New York 12180-3590

Received April 8, 1998; revised April 5, 1999

A new artificial viscosity (Q) model, based on physical conservation corrections for momentum, and a new artificial heat transfer (H) formulation are developed for the analysis of one-dimensional compressible fluid transients in plane, cylindrical, and spherical geometries. The accuracy of these formulations is verified against various benchmark shock tube problems. A Q-induced geometric error for cylindrical and spherical geometry is defined and the benefits of the Q formulation presented are demonstrated. It is also shown that these formulations can control the total variation of the solution and have superior shock-capturing capabilities. Comparisons are made with the original Q formulations of J. von Neumann and R. D. Richtmyer (1950, *J. Appl. Phys.* **21**, 232), W. F. Noh's $Q\&H$ shock-following method (1987, *J. Comput. Phys.* **72**, 78), and the piecewise-parabolic method of P. Colella and P. R. Woodward (1984, *J. Comput. Phys.* **54**, 174). The comparisons demonstrate the advantages of the new method. Numerical examples for more realistic equations of state which show the robustness of the method are also presented.

Key Words: numerical filters; artificial viscosity; artificial heat transfer; momentum correction; energy correction; Lagrangian hydrodynamics; shocks.

1. INTRODUCTION

The development of numerical methods for solving systems of nonlinear hyperbolic conservation equations that have sharp discontinuities in the solutions is a major objective in fluid dynamics. Indeed, during the last several decades, numerous methods have been developed. Perhaps the most popular method is that of von Neumann and Richtmyer [1], which uses finite difference techniques combined with so-called artificial viscosity. This method is simple to use and is economical to apply. Unfortunately, the results using this method smear shocks, and serious errors can be induced by using artificial viscosity for the calculation of strong shocks. More recently Engquist filters [2] were used to improve computational

0021-9991/99 $30.00

efficiency. This method can be easily implemented into existing codes because the filter step is essentially independent of the basic differencing scheme. Nevertheless, an increase in run time is required due to an additional filter step which contains field-by-field decomposition. In addition to the above mentioned methods, a variety of shock-capturing schemes have been developed to improve resolution of the shock and the accuracy of the numerical scheme [3–11]. Many of these methods can be characterized as higher order Godunov methods, or total variation diminishing (TVD) methods. The oscillations behind a shock are eliminated by enforcing monotonicity by limiting the range of the solution (Godunov methods) or by limiting the magnitude of the fluxes in the numerical solution (TVD methods).

In selecting one of the methods for application to a specific class of problems, various things must be considered, including equations of state, geometry (e.g., cartesian, cylindrical, or spherical), boundary conditions (i.e., fixed or moving), desired computing time and acceptable accuracy, suitability of moving mesh methods, ease of implementation, and so on. When the physics is complicated, the artificial viscosity method is one of the most attractive candidates for dealing with shocks. As a consequence, in recent years, improved artificial viscosity formulations have appeared in the literature. Most of these methods attempt to overcome the disadvantages related to the errors induced by artificial viscosity (e.g., artificial heating during the reflection of strong shocks, shockless heating, and the errors which occur when shocks are propagated over a nonuniform mesh and in spherical geometry). Donat and Marquina [12] addressed the overheating problem near the wall with Godunov type schemes, and proposed an alternative flux formula to reduce pathological behavior in the numerical solutions. In the interaction of shock waves, the type of error that occurs in wall heating was found by Menikoff [13].

Noh [14] demonstrated that artificial heat transfer, H, in addition to artificial viscosity, Q, is an effective way to eliminate excess heating error during reflection of a shock. In spherical geometry, Schulz and Whalen's artificial viscosity tensor formulations of the hydrodynamic equations with Noh's H formulation were proven to be fairly accurate [14]. Other forms of artificial viscosity are based on the TVD limiter idea [15], in which the magnitude of the artificial viscosity is controlled. In particular, artificial viscosity is turned off when there is adiabatic compression without shocks and is turned on to reduce oscillations behind the shock front. Morris and Monaghan [16] used the idea of artificial viscosity with a time-varying coefficient in their smoothed particle hydrodynamics (SPH) method to reduce smearing of shocks and vorticity decay. In their work, artificial viscosity evolves according to a simple source and decay equation. The amount of artificial viscosity increases when a fluid particle enters a shock and the decay term causes it to decay to a small value beyond the shock. These formulations of artificial viscosity can give greater accuracy than von Neumann's original formulation; however, the improvement in accuracy is restricted to specific classes of problems and thus these methods are not fully satisfactory.

The objective of this paper is to present and test a new artificial viscosity (Q) and artificial heat transfer (H) formulation which contains properties of a nonlinear filter. These formulations of Q and H were developed by considering the physical meaning of artificial viscosity and artificial heat transfer in the finite difference equations over a staggered one-dimensional mesh. It is interesting to note that for slab symmetry, our Q formulation reduces to the artificial viscosity formulation of von Neumann, but it is different for cylindrical and spherical geometries. In the region of oscillations, they can be diminished by intensifying the Q and H in a specified manner. Section 2 of this paper presents the basic conservation equations in Lagrangian form, followed by the corresponding finite difference equations constructed

on a staggered grid. In Section 3, we present the procedure used for the development of the H and Q corrections. Section 4 contains numerical results for Noh's constant velocity shock problem. The numerical results are compared with exact solutions, including Noh's $Q\&H$ shock-following method and the piecewise-parabolic method (PPM) of Colella and Woodward [17]. Shock problems for real equations of state are also considered, to demonstrate the robustness of the method. The final section contains the salient conclusions of our work.

2. LAGRANGIAN HYDRODYNAMICS WITH ARTIFICIAL VISCOSITY, *Q*, AND ARTIFICIAL HEAT TRANSFER, *H*

The conservation equations in Lagrangian form are:

Mass conservation

$$v = \frac{1}{\rho} = \left(\frac{1}{\alpha+1}\right)\frac{\partial(r^{\alpha+1})}{\partial m}, \tag{1}$$

Momentum conservation

$$\frac{\partial u}{\partial t} = -r^{\alpha}\frac{\partial(p+Q)}{\partial m}, \tag{2}$$

Energy conservation

$$\frac{\partial \varepsilon}{\partial t} = -(p+Q)\frac{\partial v}{\partial t} + \frac{\partial H}{\partial m}. \tag{3}$$

Finally, the spatial coordinate, $r(m,t)$, satisfies the ordinary differential equation

$$\frac{dr}{dt} = u(m,t). \tag{4}$$

Here the corrections Q and H are to be specified, and v is the specific volume, ρ is the density (v^{-1}), u is the velocity, ε is the specific internal energy, p is the pressure, t is time, and α is either 0, 1, or 2, depending on whether there is planar, cylindrical, or spherical symmetry, respectively. The equation of state in general form is $p = p(\varepsilon, v)$. For the special case of an ideal gas, the equation of state is $p = (\gamma-1)\rho\varepsilon$, where γ, the ratio of specific heats, is assumed to be greater than unity. The independent Lagrangian variables are m and t. The spatial coordinate, r, is related to the mass coordinate, m, by

$$m(r) = \int_{r_0}^{r} \rho r^{\alpha}\, dr = \int_{R_0}^{R} \rho^0 R^{\alpha}\, dR, \tag{5}$$

where R is taken as the initial position of the Eulerian coordinate (i.e., $r(R,0) = R$), and $\rho^0 = \rho(r,0)$ is the initial density. See also Fig. 1.

For the difference equations, we essentially follow the staggered mesh difference formulation given by von Neumann and Richtmyer [1]; however, in our formulation an explicit treatment of the Q and H corrections is added in the energy equation. The scalar quantities Q and H developed in this paper are physical corrections of momentum and energy so that there is no special reason for treating them implicitly.

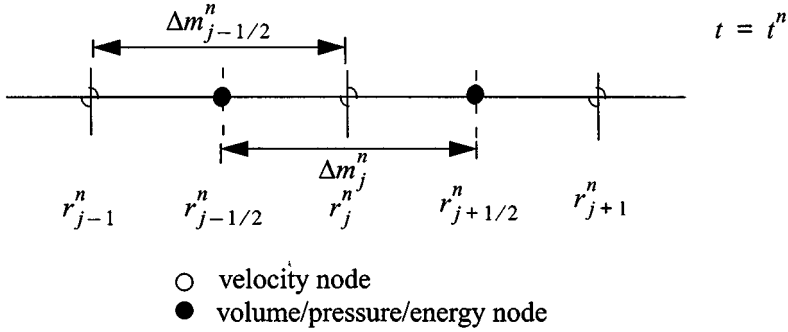

FIG. 1. Staggered grid for spatial discretization in Lagrangian coordinates.

Let

$$\Delta m_{j+1/2} = \rho^0_{j+1/2}\left(\frac{R^{\alpha+1}_{j+1} - R^{\alpha+1}_j}{\alpha+1}\right) \qquad \text{and} \qquad \Delta m_j = \frac{1}{2}(\Delta m_{j-1/2} + \Delta m_{j+1/2});$$

then

$$u^{n+1}_j = u^n_j - \frac{\Delta t}{\Delta m_j}(r^n_j)\left(p^n_{j+1/2} + Q^n_{j+1/2} - p^n_{j-1/2} - Q^n_{j-1/2}\right), \tag{6}$$

$$r^{n+1}_j = r^n_j + \Delta t u^{n+1}_j, \tag{7}$$

$$v^{n+1}_{j+1/2} = \frac{1}{\Delta m_{j+1/2}}\left(\frac{\left(r^{\alpha+1}_{j+1}\right)^{n+1} - \left(r^{\alpha+1}_j\right)^{n+1}}{\alpha+1}\right), \tag{8}$$

$$\tilde{\varepsilon}^{n+1}_{j+1/2} = \varepsilon^n - \left(p^n_{j+1/2} + Q^n_{j+1/2}\right)\left(v^{n+1}_{j+1/2} - v^n_{j+1/2}\right) + \frac{\Delta t}{\Delta m_{j+1/2}}\left(H^n_{j+1} - H^n_j\right), \tag{9}$$

$$p^{n+1}_{j+1/2} = p\left((\tilde{\varepsilon})^{n+1}_{j+1/2}, v^{n+1}_{j+1/2}\right), \tag{10}$$

$$\varepsilon^{n+1}_{j+1/2} = \varepsilon^n - \frac{\left(p^{n+1}_{j+1/2} + p^n_{j+1/2}\right)}{2}\left(v^{n+1}_{j+1/2} - v^n_{j+1/2}\right) + \frac{\Delta t}{\Delta m_{j+1/2}}\left(H^n_{j+1} - H^n_j\right). \tag{11}$$

3. *Q* AND *H* FORMULATIONS

The basic Q and H formulations were developed as physical conservation corrections for momentum and energy, respectively. Thus the properties of a nonlinear filter are easily added in the formulations of Q and H by simply intensifying the corrections of momentum and internal energies at a few mesh points where Gibbs oscillations occur.

3.1. *The* Basic *Q Formulation*

Mathematically, the differential form of the equations is obtained from integral equations representing conservation laws, with the assumption that the physical solution is smooth. In a region of rapid change, the smoothness assumption is difficult to realize with a finite difference approximation. A finite difference treatment of pressure shocks without Q gives an unrealistically overestimated node velocity. Artificial viscosity in the problems involving

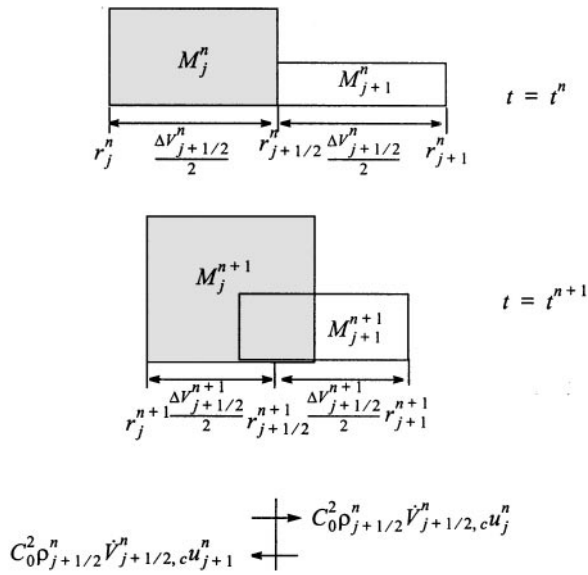

FIG. 2. Schematic diagram of the momentum correction procedure.

a strong shock must be used in such a way as to correct the nonphysical velocity induced by treating the discontinuity with a finite difference approximation. In particular, adding a certain amount of artificial viscosity in the momentum equation as a way to achieve solutions as accurate as high resolution (non-Q) schemes implies that the artificial viscosity formulation can be interpreted as an approximate Riemann solver [15]. An artificial viscosity formulation can also be interpreted as a nonlinear filter. Indeed, the success of the method depends on finding an accurate formulation of artificial viscosity which contains these properties. The momentum equation without Q can be expressed as

$$u_j^{n+1} = u_j^n - \frac{\Delta t}{\Delta m_j}\left(r_j^n\right)^{\alpha}\left(p_{j+1/2}^n - p_{j-1/2}^n\right). \tag{12}$$

We have developed an artificial viscosity formulation which has physical meaning based on Eq. (12). In particular, the compression of the node after one time step can be regarded as overlapping the two nearest mass-weighted average velocities; see Fig. 2. In other words, mixing of momentums occurs in the volume node undergoing compression.

In this paper, the amount of momentum transfer due to the mixing of momentums is given as a momentum correction because the term involves a filtering procedure which is independent of the difference scheme. The amount of this momentum correction is related also to the artificial viscosity formulation. The momentum transfer rate by the momentum mixing in node $j + 1/2$ is given by

$$\dot{M}_{j+1/2}^n = C_0^2 \Delta \dot{m}_{j+1/2,c}^n \left(u_j^n - u_{j+1}^n\right), \tag{13}$$

where C_0^2 is a dimensionless constant and $\Delta \dot{m}_{j+1/2,c}^n$ is the mass mixing rate due to the volume compression in node $j + 1/2$,

$$\Delta \dot{m}_{j+1/2,c}^n = \rho_{j+1/2}^n \dot{V}_{j+1/2,c}^n \qquad \text{if } \dot{V}_{j+1/2,c}^n > 0, \tag{14}$$

and $\dot{V}^n_{j+1/2,c}$ is the volume compression or expansion rate,

$$\dot{V}^n_{j+1/2,c} = \left(r^n_{j+1/2}\right)^\alpha \left(u^n_j - u^n_{j+1}\right). \tag{15}$$

In the case of an expansion, $\dot{V}^n_{j+1/2,c} \le 0$, there is no mixing; thus $\Delta\dot{m}^n_{j+1/2,c} = 0$. As seen in Fig. 2, when $C_0^2 = 2$, the artificial momentum transfer is carried by the whole mass in the mixing region. After a correction due to the momentum mixing is added in Eq. (13), the final amounts of momentum contained in the left-hand-side half volume and the right-hand-side half volume, at $j + 1/2$ and t^{n+1}, are

$$M^{n+1}_{j+1/2,l} = 0.5\Delta m_{j+1/2} u^{*n+1}_j - \Delta t \dot{M}^n_{j+1/2} \tag{16}$$

and

$$M^{n+1}_{j+1/2,r} = 0.5\Delta m_{j+1/2} u^{*n+1}_{j+1} + \Delta t \dot{M}^n_{j+1/2}, \tag{17}$$

respectively. Here u^{*n+1}_j is the result obtained without a momentum correction. As can be noted in Eqs. (16) and (17), the total amount of momentum during the integration step is conserved in the process of the momentum correction. After the same approach is applied to the other side, the final corrected mass-weighted average velocity is

$$u^{n+1}_j = \frac{M^{n+1}_{j-1/2,r} + M^{n+1}_{j+1/2,l}}{\Delta m_j} = u^{*n+1}_j + \frac{\Delta t\left(\dot{M}^n_{j-1/2} - \dot{M}^n_{j+1/2}\right)}{\Delta m_j}. \tag{18}$$

With artificial viscosity added, Eq. (12) can be rewritten as

$$u^{n+1}_j = u^{*n+1}_j - \frac{\Delta t}{\Delta m_j}\left(r^n_j\right)^\alpha \left(Q^n_{j+1/2} - Q^n_{j-1/2}\right). \tag{19}$$

Conceptually, Eq. (19) is equivalent to Eq. (18). Thus the artificial viscosity formulation derived from the process of the momentum conservation correction is given by

$$Q^n_{j-1/2} - Q^n_{j+1/2} = \frac{\dot{M}^n_{j-1/2} - \dot{M}^n_{j+1/2}}{\left(r^n_j\right)^\alpha}. \tag{20}$$

Summing Eq. (20) from node j to boundary node $j = N$, and assuming that the amounts of momentum correction ($\dot{M}^n_{N+1/2}$) and artificial viscosity ($Q^n_{N+1/2}$) in the boundary nodes are zero, we find that the general Q formulation for plane, cylindrical, and spherical geometries is

$$Q^n_{j-1/2} = \sum_{l=j}^{N} \left(\frac{\dot{M}^n_{l-1/2} - \dot{M}^n_{l+1/2}}{\left(r^n_l\right)^\alpha} \right). \tag{21}$$

One of the main reasons for using artificial viscosity in a numerical method is that one can properly handle shocks by distributing the momentum near a discontinuity. However,

the overall amount of momentum must not be changed by using artificial viscosity. In other words, the artificial viscosity cannot be a momentum source. This is the reason why the summation in Eq. (21) must be used in the Q formulation for cylindrical and spherical geometries. In contrast, for plane geometry, the momentum correction terms of other volume nodes on the right-hand side of Eq. (21) cancel out after summation because $(r_l^n)^\alpha = 1$ at every velocity node. Thus the artificial viscosity is simply related to the amount of the momentum correction in each volume node,

$$Q_{j-1/2}^n = \dot{M}_{j-1/2}^n = C_0^2 \rho_{j-1/2}^n \left(u_{j-1}^n - u_j^n\right)^2. \tag{22}$$

We note that Eq. (21) is identical to the Q formulation given by von Neuman and Richtmyer [1] for plane geometry, but not for cylindrical and spherical geometries.

3.2. *The* Filtered *Q and H Formulations*

As one can see in Eq. (21), the Q formulation is accomplished by determining the momentum correction ($\dot{M}_{j+1/2}^n$) in each volume node. In the compression nodes, $\dot{M}_{j+1/2}^n$ is given by Eq. (13). Whenever $\dot{M}_{j+1/2}^n \neq 0$, we have

$$\left|u_{j+1}^{n+1} - u_j^{n+1}\right| < \left|u_{j+1}^{*n+1} - u_j^{*n+1}\right|. \tag{23}$$

Thus Q contains a total variation diminishing property that adjusts $\dot{M}_{j+1/2}^n$. When an overshoot of pressure is introduced into the node, Eq. (13) is replaced by

$$\dot{M}_{j+1/2}^n = C_1 \frac{\Delta m_{j+1/2}}{\Delta t}\left(u_j^n - u_{j+1}^n\right), \tag{24}$$

where C_1 is a dimensionless constant that intensifies the momentum correction. The two velocities u_j^{n+1} and u_{j+1}^{n+1} cannot be overcompensated so that a new extremum is created. The maximum value allowed for C_1 is 0.25, which makes $M_{j+1/2,l}^{n+1} = M_{j+1/2,r}^{n+1}$ after the momentum correction using Eqs. (16) and (17).

For the development of the artificial heat transfer formulation (H), we have used the same approach as that used for the Q formulation. The H formulation is only used in a region of compression ($\rho(r,t)/\rho^0 > 1$), where H is the amount of the energy transfer due to the mixing of internal energy at velocity node j, induced by compressions in adjacent volume nodes. Thus, the filtered H is analogous to the filtered Q:

$$H_j^n = C_1 \left(\frac{\Delta m_{j-1/2} + \Delta m_{j+1/2}}{2\Delta t}\right)\left(\varepsilon_{j-1/2}^n - \varepsilon_{j+1/2}^n\right). \tag{25}$$

A method for detecting undesirable maximums and their corrections for systems of equations was described by Engquist [2]. Using Eqs. (24) and (25), we present a filtering procedure for our system of equations in a pseudo-language algorithm, which corresponds to the implementation of the nonlinear filtering, artificial viscosity, and heat transfer corrections discussed above.

3.3. *The Filtering Algorithm*

Assume that n time steps have been computed. To calculate the needed filtering, artificial viscosity, and heat transfer corrections for the calculation of advanced time level results, we perform the following calculations, where Δ_+ and Δ_- are the forward and backward differences, respectively, $\Delta_\pm u_j = \pm(u_{j\pm1} - u_j)$:

Do $j = 0, N-1$
$j_{filter,Q} = 0$, $j_{filter,H} = 0$.
If, $j = 0$, **then**, $\Delta_- u_j = -\Delta_+ u_j$, $\Delta_- \rho_{j+1/2} = 0$, $\Delta_- \varepsilon_{j+1/2} = 0$
If, $j = N-1$, **then**, $\Delta_+ u_{j+1} = 0$, $\Delta_+ \rho_{j+1/2} = 0$, $\Delta_+ \varepsilon_{j+1/2} = 0$
If, $[(\Delta_+ u_j)(\Delta_- u_j) < 0$, **and**, $(\Delta_+ u_{j-1})(\Delta_- u_{j+1}) < 0]$, **or**,
$[(\Delta_+ \rho_{j+1/2})(\Delta_- \rho_{j+1/2}) < 0$, **and**, *not admissible* $(j, \rho^n, \rho^{n-1})]$, **then**,
$j_{filter,Q} = 1$
Endif
If, $(\Delta_- \varepsilon_{j+1/2})(\Delta_- \rho_{j+1/2}) < 0$, **or**,
$[(\Delta_+ \varepsilon_{j+1/2} + \Delta_- \varepsilon_{j+1/2})\Delta_- \varepsilon_{j+1/2} < 0$, **and**, *not admissible* $(j, \varepsilon^n, \varepsilon^{n-1})$, **then**,
$j_{filter,H} = 1$
Endif
Enddo
Do $j = 0, N-1$
If, $j_{filter,Q} = 0$, **then**,
$\dot{M}_{j+1/2} = C_0^2 \Delta \dot{m}_{j+1/2,c}(u_j - u_{j+1})$ [if a Lagragian formulation]
$\dot{M}_{j+1/2} = C_0^2 \left(\frac{\Delta R_{max}}{\Delta r_{j+1/2}}\right)^2 \Delta \dot{m}_{j+1/2,c}(u_j - u_{j+1})$ [if an Eulerian formulation]
Else
$\dot{M}_{j+1/2} = C_1 \frac{\Delta m_{j+1/2}}{\Delta t}(u_j - u_{j+1})$
Endif
Enddo
$Q_{N+1/2} = 0$, $\dot{M}_{N+1/2} = 0$.
Do $j = N, 1, -1$
$Q_{j-1/2} = Q_{j+1/2} + (\dot{M}_{j-1/2} - \dot{M}_{j+1/2})/(r_j)^\alpha$
Enddo
$H_0 = 0$, $H_N = 0$.
Do $j = 1, N-1$
$H_j = 0$
If, $\rho^n_{j-1/2} / \rho^0_{j-1/2} > 1$, **and**, $\left(\rho^n_{j+1/2} / \rho^0_{j+1/2}\right) > 1$, **then**,
If, $j_{filter,H} = 1$, **or**, $[j - 1_{filter,H} = 1$, **and**, $j + 1_{filter,H} = 1]$, **then**,
$H_j = C_1\left(\frac{\Delta m_{j-1/2} + \Delta m_{j+1/2}}{2\Delta t}\right)(\varepsilon_{j-1/2} - \varepsilon_{j+1/2})$
Else
If, $j + 1_{filter,H} = 1$, **then**,
$H_j = C_1\left(\frac{\Delta m_{j+1/2}}{2\Delta t}\right)(\varepsilon_{j-1/2} - \varepsilon_{j+1/2})$
Elseif, $j - 1_{filter,H} = 1$, **then**,
$H_j = C_1\left(\frac{\Delta m_{j-1/2}}{2\Delta t}\right)(\varepsilon_{j-1/2} - \varepsilon_{j+1/2})$
Endif
Endif
Endif
Enddo

Function *admissible* (j, ρ^n, ρ^{n-1})

If, $\min\left(\rho^{n-1}_{j-1/2}, \rho^{n-1}_{j+1/2}, \rho^{n-1}_{j+3/2}\right) < \rho^n_{j+1/2} < \max\left(\rho^{n-1}_{j-1/2}, \rho^{n-1}_{j+1/2}, \rho^{n-1}_{j+3/2}\right)$, **then**,
true
Else
false
Endif

Return

4. NUMERICAL TESTS

In order to assess the performance of the artificial viscosity and artificial energy transfer formulations discussed above, we chose problems involving shock waves, contact discontinuities, and the reflection of strong shocks at a wall, or at the geometric center of spherical geometries, to allow verification against known analytical solutions of the equations being modeled. The Eulerian Q formulations are the same as the Lagrangian Q formulations, Eq. (21), except for the dimensionless constant. We note that the dimensionless constants for Lagrangian and Eulerian formulations, C_0^2 and $C_{0,E}^2$, are related by the *Jacobian*, $J = \frac{\partial r}{\partial R}$, $C_{0,E}^2 = C_0^2(\frac{\partial R}{\partial r})^2$. Therefore the amount of momentum correction for an Eulerian formulation of artificial viscosity is

$$\dot{M}^n_{j+1/2} = C_0^2 \left(\frac{\Delta R_{\max}}{\Delta r^n_{j+1/2}} \right)^2 \Delta \dot{m}^n_{j+1/2,c} \left(u^n_j - u^n_{j+1} \right). \tag{26}$$

The meaningful range of the dimensionless constants for the Q and H formulations found in Section 3 are $0.0 \le C_0^2 \le 2.0$ and $0.0 \le C_1 \le 0.25$. The C_1 value used for all our numerical tests was 0.25. We found that the dependency of the numerical solutions on the magnitude of C_1 was negligible. The magnitude of this constant affects the speed of correction for the nonphysically determined variables but does not affect the final solutions significantly. As can be seen in Fig. 3, the numerical results are also not strongly dependent on the magnitude of C_0^2. The stability limit must satisfy a Courant condition [18], as for other Q explicit methods. In order to effectively eliminate the oscillations using a filter Q correction, we need one more condition for every node:

$$C_0^2(|\Delta u_{j-1/2}| + |C_{s,j-1/2}|)\rho_{j-1/2} \le C_1 \frac{\Delta m_{j-1/2}}{\Delta t}. \tag{27}$$

Numerical calculations were carried out in this study using the following time step to assure these conditions:

$$\Delta t = \min\left(\frac{0.5 C_1 \Delta r_{j-1/2}}{|\Delta u_{j-1/2}| + |C_{s,j-1/2}|} \right). \tag{28}$$

For simplicity, we have used some specific notation to identify each method. In particular,

$$B\text{-}Q\&H_{L \text{ or } E}\left(C_0^2\right)$$

denotes our Lagrangian $Q\&H$ or our Eulerian $Q\&H$ formulation, respectively, each of which contains filtering properties. Similarly,

$$N\text{-}Q\&H_{L \text{ or } E}\left(C_0^2, C_1, h_0^2, h_1\right)$$

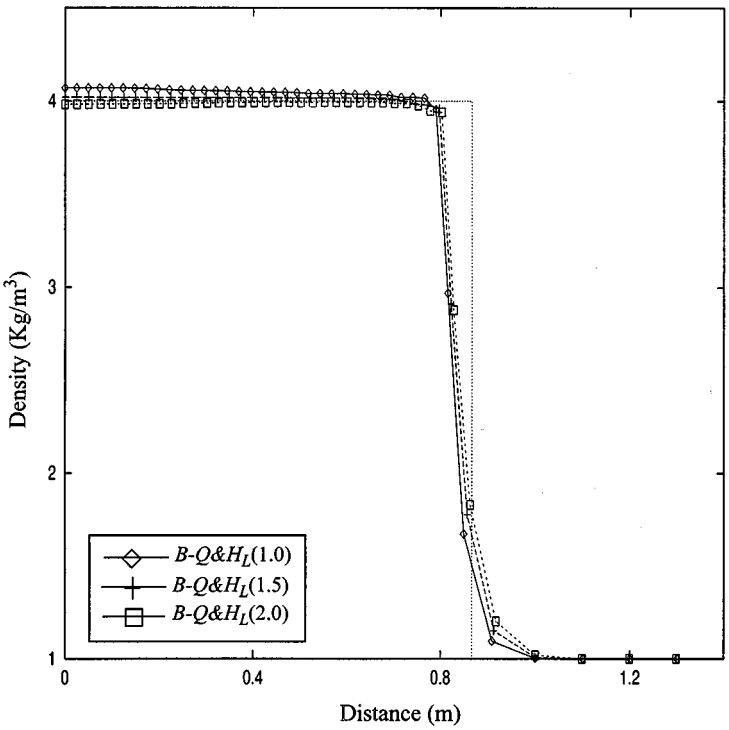

FIG. 3. The dependence of solutions on the parameter, C_0^2.

denotes Noh's Lagrangian $Q\&H$ or Noh's Eulerian $Q\&H$ formulation [14], respectively. Similarly, $Q_o(C_0^2)$ and $B\text{-}Q(C_0^2)$ denote the original Q method of von Neumann and Richtmyer and our Lagrangian Q formulation which does not contain filtering properties, respectively, where C_0^2, C_1, h_0^2, and h_1 are the dimensionless coefficients used to obtain the numerical results with each method.

4.1. *Noh's Shock Wave Problems*

In our first series of tests we study Noh's three shock wave problems [14], which differ only in their spatial symmetries. These are well known, very severe tests for Q methods with which to check for Q-induced errors. The initial conditions are $\rho(r, 0) = 1$, $p(r, 0) = 0$, $\varepsilon(r, 0) = 0$, and $u(r, 0) = -1$, except at the origin, where it must be zero. The equation of state used was that for an ideal gas with $\gamma = 5/3$. For this case, shock waves generated at the origin propagate with a constant velocity of $1/3$, and the internal energy behind the shock is 0.5 and the densities are 4, 16, and 64 for plane, cylindrical, and spherical geometries, respectively.

4.1.1. Uniform mesh in plane geometry. The results for plane symmetry used to study the sensitivity of our numerical method to the constant of C_0^2 are shown in Fig. 3, where density is plotted versus the distance. The results are all shown for 40 cells ($\Delta R = 0.1$) at $t = 2.6$. The effectiveness of the filter Q developed in this paper as a tool with which to suppress numerical oscillation is apparent. We see that the wall heating error [14] is effectively eliminated using the filtered artifical heat transfer formulation. The numerical results with zero wall heating error are obtained using $B\text{-}Q\&H_L(1.5)$. The wall heating

error was about 1.7% for $C_0^2 = 1$. The use of artificial heat transfer to eliminate the wall heating error is well known [14]. The main disadvantage of previous artificial heat transfer formulations was considerable smearing of the shock front when a given amount of artificial viscosity was used. The smearing of the shock with the current artificial heat transfer formulation is small, about a half mesh interval, and the shock discontinuity is well resolved within four mesh intervals.

4.1.2. Nonuniform mesh in plane geometry. As noted by Noh [14], classical formulations of Q produce additional Q error when shocks are propagated over a nonuniform mesh. To test the current formulations on a nonuniform mesh, we used the same nonuniform mesh as that used by Noh for studying this type of error,

$$\Delta R_{j+1} = \chi \Delta R_j, \tag{29}$$

where χ is 1.05. If χ is replaced by χ^{-1} in Eq. (29), the mesh decreases for the first half region and then increases for the second half. This type of error was discussed theoretically by Noh [14]. In fact, he verified that this type of error is unavoidable using a Lagrangian formulation of artificial viscosity because this error is already inherent in the solution of the differential equations. However, this error is related to the transient nature of the shock thickness; thus an Eulerian formulation of artificial viscosity is preferred because constant shock thickness (i.e., fixed length) can be specified.

The condition $\Delta R_{\max} \geq \Delta r_{\max}$ must be satisfied in Eq. (26). For the purpose of simulation, we may take $\Delta R_{\max} = \Delta r^0_{\max}$, which suffices for this problem. Figure 4 compares the result

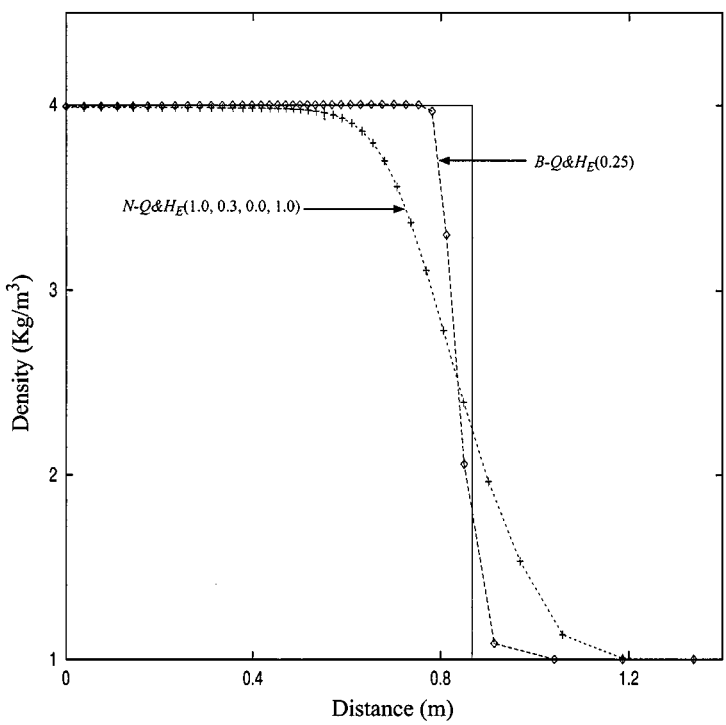

FIG. 4. The present Eulerian formulation B-Q&$H_E(0.25)$ is compared with Noh's Eulerian N-Q&$H_E(1.0, 0.3, 0.0, 1.0)$ formulation.

of the B-$Q\&H_E(0.25)$ with the Noh's $Q\&H_E(1.0, 0.3, 0.0, 1.0)$. Since a very large Q_E constant in Noh's $Q\&H$ formulations is necessary to eliminate the nonuniform error, the results obtained with these constants show spreading of the shock over a large number of the smaller zones. In a comparison of Figs. 3 and 4, a nonuniform mesh error does not appear in the B-$Q\&H_E(0.25)$ results. Note that the shock thickness is equivalent to the one obtained with a uniform mesh and the Lagrangian formulation of artificial viscosity with $C_0^2 = 1.5$. The shock is resolved in four mesh intervals in both cases by the use of a much smaller constant, C_0^2, for B-$Q\&H_E$. It is clear that the current formulations of filter $Q\&H$ permit the use of smaller C_0^2 for resolving the shock for both a uniform and a nonuniform mesh in plane symmetry.

4.1.3. Spherical geometry. The case of spherical geometry is well known to be a severe test, and a number of numerical methods fail to give correct solutions. Indeed, serious error appears in the solutions with the original Q method (i.e., up to 1000% error near the origin because of "wall heating"). This type of error was discussed by Noh [14]; he showed that it depends on the Q formulation. Thus this test problem is a crucial benchmark for our new Q formulation.

In Section 3, the unified Q formulation for plane, cylindrical, and spherical geometries was developed in such a way as to conserve the overall momentum and yield a new formulation for cylindrical and spherical geometries. Figure 5a shows the density profiles at $t = 0.6$ s for 100 cells, where the new formulation B-$Q(2.0)$ is compared with the original $Q_o(2.0)$, Noh's standard N-$Q\&H_L(2.0, 0.0, 0.0, 0.0)$, and the exact solution, $\rho = 64$, behind the shock. It can be seen that the error for the B-$Q(2.0)$ is 7% near the shock, while the errors for N-$Q\&H_L(2.0, 0.0, 0.0, 0.0)$ and $Q_o(2.0)$ are 19% and 40% near the shock, respectively. As shown in the earlier test of plane symmetry, a wall heating error is inevitable in difference solutions, since it already occurs in the exact solution of the differential equation with Q [14]. The same conclusion holds for any shock-smearing method [17]. However, the wall heating error can be eliminated using artificial heat transfer, H. The same conclusion holds for spherical geometry; however, the wall heating error shown in Fig. 5a is dependent on the Q formulation also. Figure 5b shows the velocity profiles of these results. It can be seen that there is an increased amount of momentum at the grids (maximum near the shock) with N-$Q\&H_L(2.0, 0.0, 0.0, 0.0)$ and von Neumann $Q_o(2.0)$. As noted in Section 3, in a numerical method artificial viscosity is used to properly handle the shock by distributing the momentum near the discontinuity where the total amount of momentum must be conserved. The necessary condition for doing this with a Q correction is

$$\sum_{j=-N}^{N} r_j^{\alpha} \left(Q_{j-1/2}^n - Q_{j+1/2}^n \right) = 0.0, \tag{30}$$

where $j = -N$, $j = 0$, and $j = N$ are the left-hand-side boundary node, the geometric origin, and the right-hand-side boundary node, respectively, and $\dot{M}_{-j-1/2}^n = \dot{M}_{j+1/2}^n$ because of spherical symmetry. At the boundary nodes, $Q_{\pm N\pm 1/2}^n$ and $\dot{M}_{\pm N\pm 1/2}^n$ are zero. This condition is satisfied for the new definition of Q in Eq. (21), which is expressed in terms of the momentum correction. For plane symmetry, this condition is automatically satisifed. However, no Q formulation not using a summation can satisfy the condition given by Eq. (30) for cylindrical and spherical geometries. Thus the total amount of momentum creation rate with Q, which is called the geometric error, is greater than zero. This is shown in Fig. 5d, where the geometric error for our B-$Q(2.0)$ is compared with the errors for Noh's standard

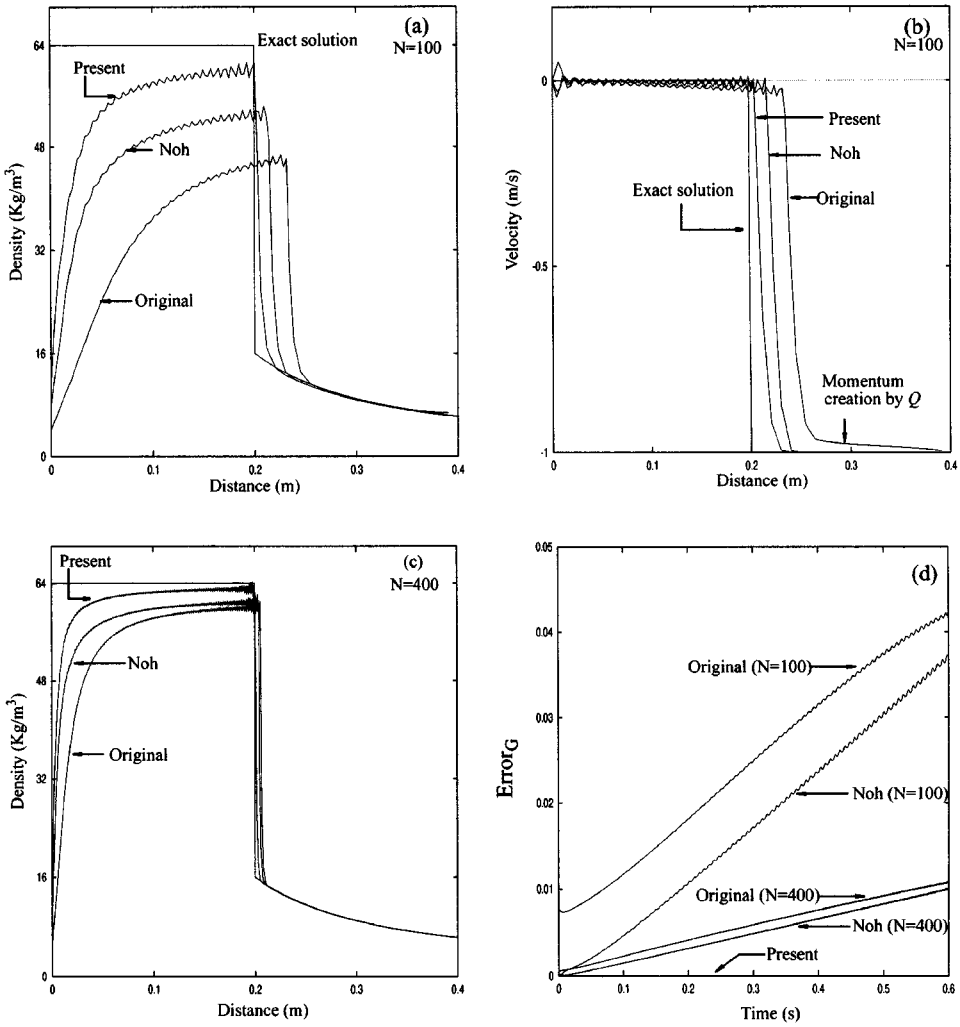

FIG. 5. The solutions for Noh's spherical shock problem with 100 cells ($\Delta R = 0.01$ m) and with 400 cells ($\Delta R = 0.025$ m), profiles for density and velocity in (a, c) and (b), respectively. The transient geometric error is shown in (d). Here we compare the present B-$Q(2.0)$ with Noh's N-$Q\&H_L(2.0, 0.0, 0.0, 0.0)$ and the original $Q_o(2.0)$ of von Neumann. The geometric error is defined by the amount of momentum created by Q formulation, which is given by $\text{Error}_G(t^n) = \sum_{j=-N}^{N} (r_j^n)^\alpha (Q_{j-1/2}^n - Q_{j+1/2}^n)$.

N-$Q\&H_L(2.0, 0.0, 0.0, 0.0)$ and the original $Q_o(2.0)$. Using B-$Q(2.0)$, zero geometric error is shown. In contrast, the geometric errors for both N-$Q\&H_L(2.0, 0.0, 0.0, 0.0)$ and $Q_o(2.0)$ grow with time. Thus the pre-shock density and velocity profiles are spread over greater and greater distances (see Figs. 5a and 5b) with increased geometric error.

We confirm this in Figs. 5c and 5d, where we show that improved results for N-$Q\&H_L(2.0, 0.0, 0.0, 0.0)$ and $Q_o(2.0)$ can be obtained by reducing the geometric error using a fine mesh interval ($N = 400$, $\Delta R = 0.0025$). Figure 5c shows the convergence of solutions for the N-$Q\&H_L(2.0, 0.0, 0.0, 0.0)$ and $Q_o(2.0)$, and Fig. 5d shows that the geometric errors are reduced using a fine mesh interval. Using $N = 400$, the numerical results with N-$Q\&H_L(2.0, 0.0, 0.0, 0.0)$ and $Q_o(2.0)$ are nearly equivalent due to the small difference in geometric error, as shown in Fig. 5d. It is clear that this error can also be reduced by

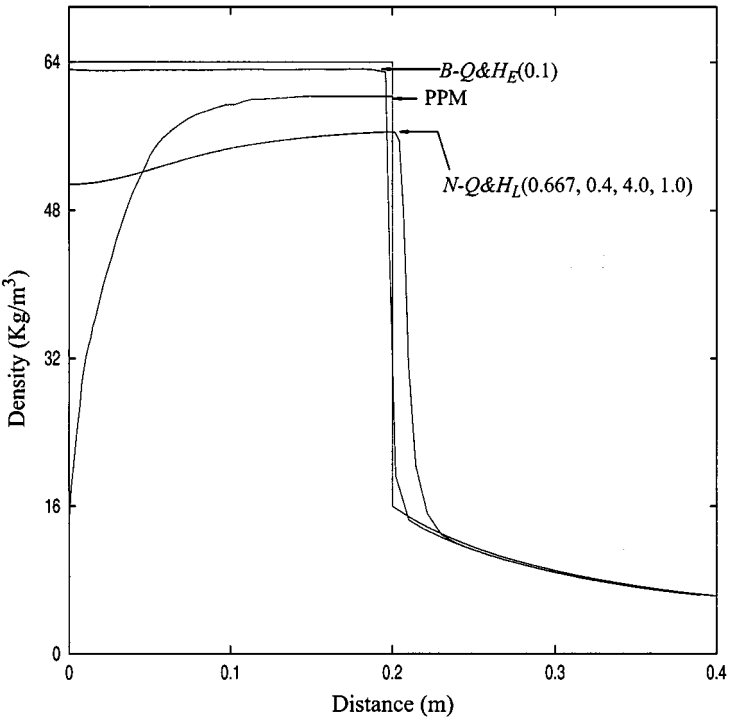

FIG. 6. Comparison of the results obtained with the present B-$Q\&H_E(0.1)$, Noh's N-$Q\&H_L(0.667, 0.4, 4.0, 1.0)$, and the (non-$Q$) PPM, with 100 cells for the final time $t = 0.6$ s.

using a smaller Q. However, the amount of error is still troublesome and this error cannot be eliminated using this kind of Q formulation. It is one of the main reasons why a numerical method with Q usually fails to obtain the correct result in cylindrical and spherical geometries. Using the formulation presented herein, the dependence of the geometric error on mesh size and Q is zero. We stress the importance of conservation of total momentum using the new formulation of Q for both cylindrical and spherical geometries.

As noted previously, the wall heating error near the origin can be eliminated using artificial heat transfer, H. This is shown in Fig. 6, where the result with B-$Q\&H_E(0.1)$ is compared with Noh's N-$Q\&H_L(0.667, 0.4, 4.0, 1.0)$ and the (non-Q) PPM technique of Colella and Woodward [17]. Superior results are obtained by the method proposed herein, and the wall heating error and the oscillation are eliminated. The same quality of solution can be obtained with B-$Q\&H_L(0.25)$. These are all shown with 100 cells at $t = 0.6$ s. In Fig. 7, B-$Q\&H_E(0.1)$ with uniform 200 cells produces essentially the converged exact solution.

4.2. *Sod's Shock Tube*

Another good test problem is due to Sod [19], and consists of two different material states separated by a diaphragm. That is:

$$(p_L, \rho_L, u_L) = (1.0, 1.0, 0.0), \text{ if } r < 0$$

and

$$(p_R, \rho_R, u_R) = (0.1, 0.125, 0.0), \text{ if } r > 0.$$

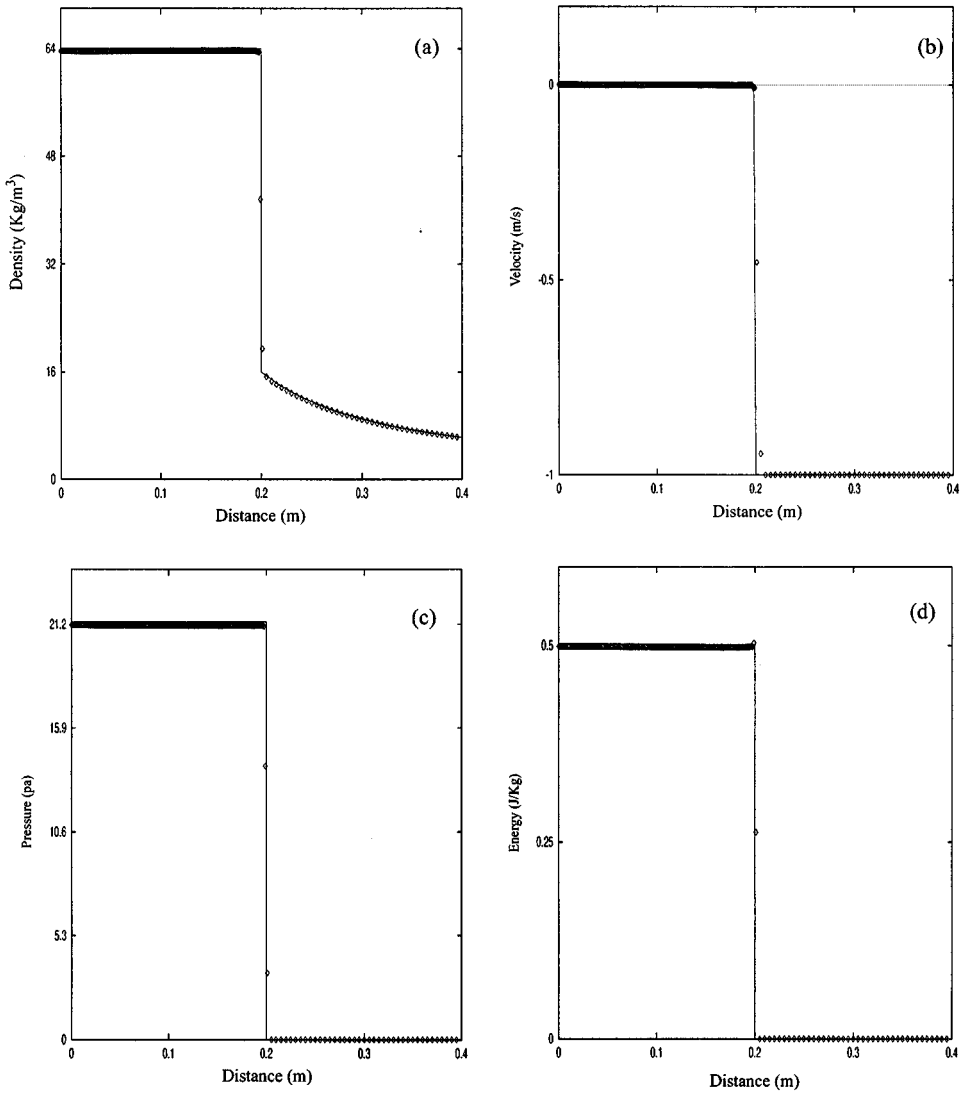

FIG. 7. The solutions for Noh's spherical shock problem with 200 cells ($\Delta R = 0.0025$ m) and B-$Q\&H_E(0.1)$ at the final time $t = 0.6$ s. Profiles for density, velocity, pressure, and internal energy are shown in (a), (b), (c), and (d), respectively.

The diaphragm is caused to rupture at time $t = 0$. After the diaphragm bursts, a shock wave moves toward the right and a rarefaction wave moves toward the left. Figure 8 shows the results at $t = 0.2$ s with 200 cells and B-$Q\&H_L(1.5)$ for a specific heat ratio $\gamma = 1.4$. The magnitudes of the various plateaus are reproduced very well without numerical oscillations. Moreover, the numerical results show that the current $Q\&H$ formulation gives the correct positions of shock waves and contact discontinuities. In fact, the sharp contact discontinuities are resolved within one mesh interval and the shocks within three mesh intervals, which compare very well with numerical results obtained using high resolution schemes [6] and modern upwind methods [11].

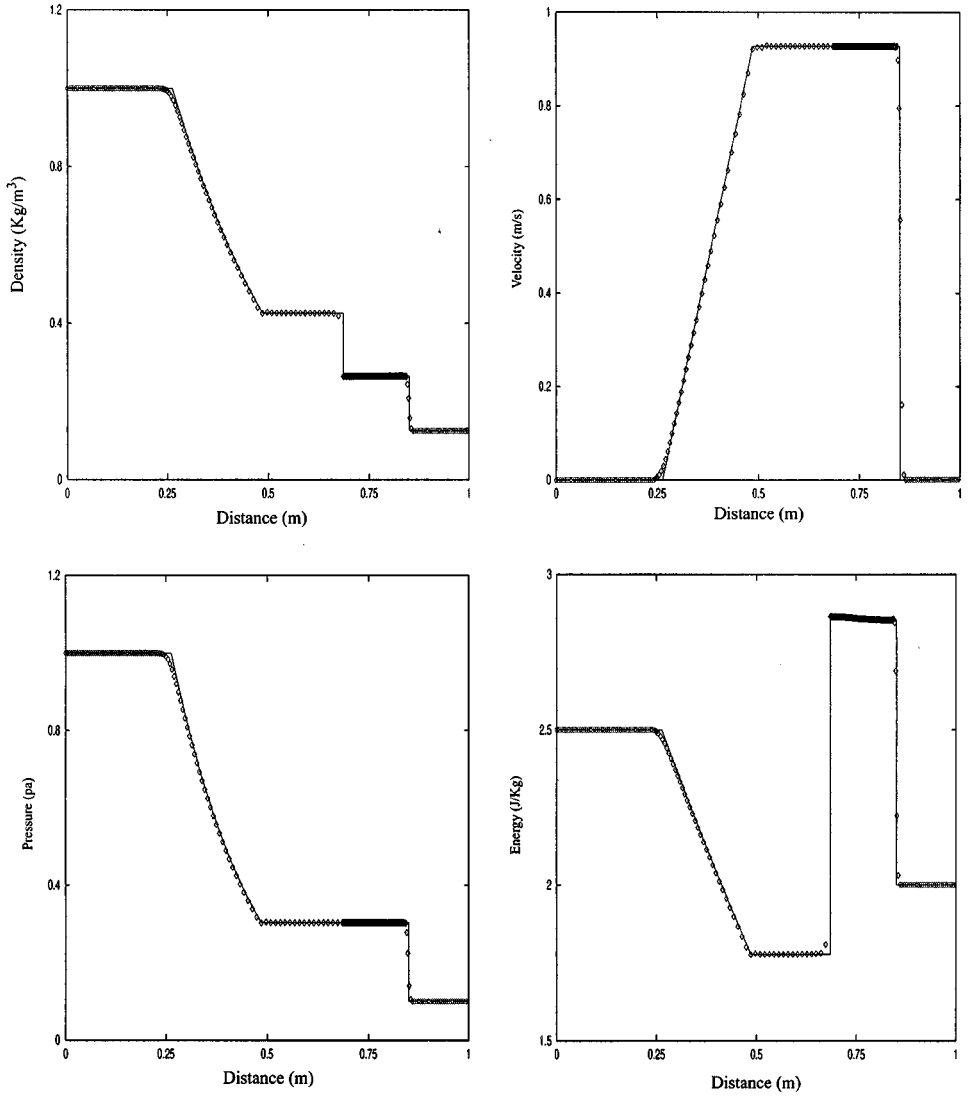

FIG. 8. The solutions for Sod's shock tube problem with 200 cells ($\Delta x = 0.005$ m) and B-$Q\&H_L(1.5)$ at $t = 0.2$ s.

4.3. *A Shock Reflection Problem Using Real Equations of State*

In this test, we considered the shock reflection problem again using a so-called general equation of state in plane symmetry. This general equation of state [20] can be written in the form

$$p = [1/(E + \phi_0)]\{\zeta(a_1 + a_2|\zeta|) + E[b_0 + \zeta(b_1 + b_2\zeta) + E(c_0 + c_1\zeta)]\}, \tag{31}$$

where $E = \rho^0\varepsilon$, $\zeta = \rho/\rho^0 - 1$, and the constants, ρ^0, a_1, a_2, b_0, b_1, b_2, c_0, c_1, ϕ_0 are given by

$$\rho^0 = 8.90,\ a_1 = 4.9578,\ a_2 = 3.6884,\ b_0 = 7.4727,\ b_1 = 11.519,$$
$$b_2 = 5.5251,\ c_0 = 0.39493,\ c_1 = 0.52883 \text{ and } \phi_0 = 3.6000,$$

The initial data for the density and velocity are 8.9 and -1, respectively. The internal energy at the initial time is chosen to have an infinite pressure ratio. This problem was solved up to the time when the shock moved a distance of 0.3 m with 100 cells ($\Delta R = 0.01$ m) and B-Q&$H_L(1.5)$. An exact and a numerical solution of this problem were obtained by Glaister, using an approximate linearized Riemann solver [20]. The numerical solution using our method is compared with the exact solution in Fig. 9. A good representation of the exact solution without Q-induced error and with the correct shock speed are shown.

4.4. *A Shock Wave Problem for an Imploding Air Bubble*

The problem we consider in this test case is concerned with the dynamics of an air bubble with initial radius $a_0 = 10\ \mu$m surrounded by a spherical flask containing water, whose outer

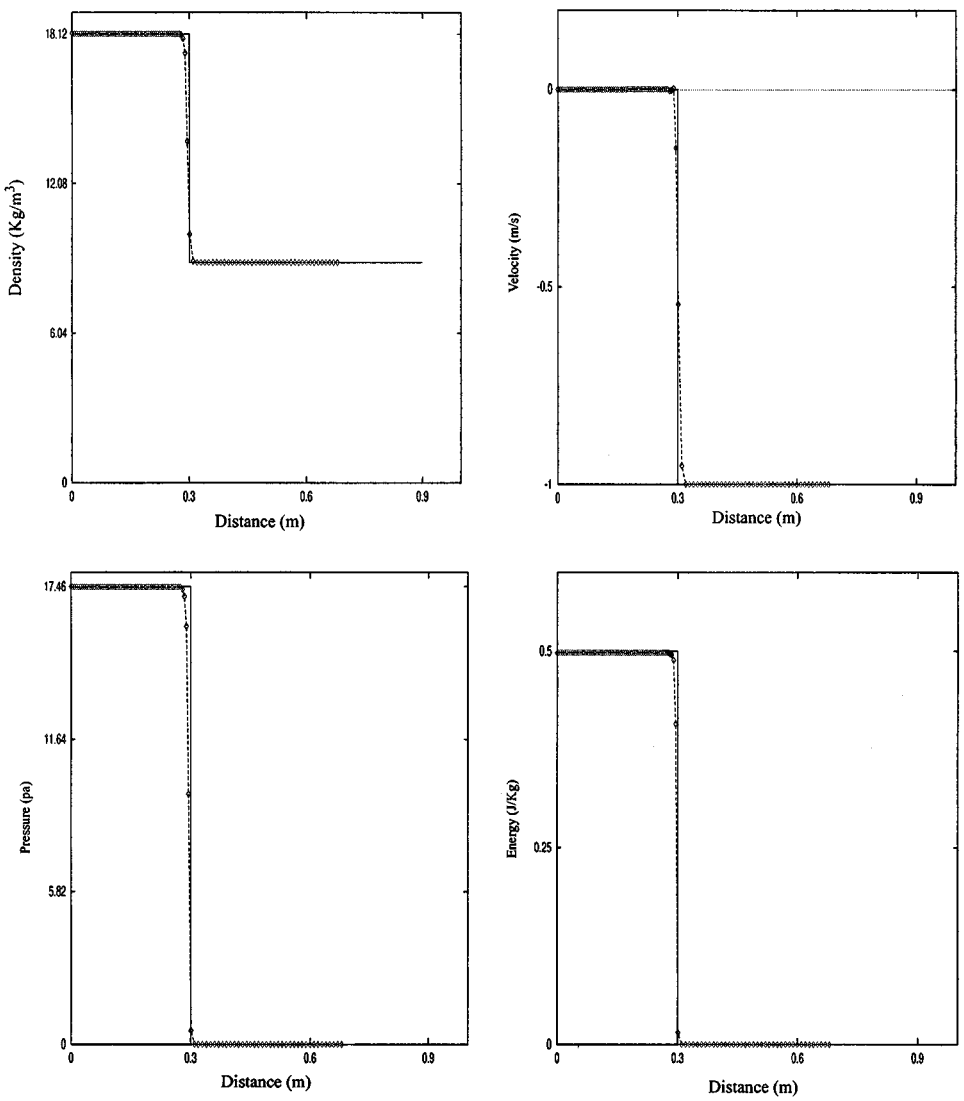

FIG. 9. The solutions for a shock reflection problem with a general equation of state; the pressure ratio $p^+/p^- = \infty$ and 100 cells ($\Delta x = 0.01$ m) for plane symmetry.

radius is $R_F = 5$ cm. The air and water are initially at atmospheric pressure, $p_0 = 1$ bar; they are in thermal equilibrium, and at rest. These parameters are typical of those found in sonoluminescence experiments.

The outer radius of the water flask is driven by an oscillatory pressure: $p_l(R_F, t) = p_0 - \Delta p \sin(2\pi f t)$. Here we used $\Delta p = 0.25$ bar and $f = 45$ kHz. The expansion of the bubble radius from its initial radius occurs on a hydrodynamic time scale during the acoustic delayed rarefaction half-cycle of the wall pressure change. This expansion brings the bubble to its maximum radius. The ensuing implosion (i.e., rapid compression) of the bubble may accelerate the air/water interface to supersonic velocities and strongly compress the gas in the bubble's interior. Moreover, it generates a strong spherically convergent shock wave. This inwardly propagating shock wave in the gas collapses to the center and rebounds.

The equation of state for air can be given by an analytic model [21] that includes vibrational excitation, dissociation, ionization, and repulsive intermolecular potentials,

$$p = R'T\rho(1 + m_D)(1 + m) + \frac{E_c \rho^0}{1 - (3/n)}\left[\left(\frac{\rho}{\rho^0}\right)^{(n/3)+1} - \left(\frac{\rho}{\rho^0}\right)^2\right], \tag{32}$$

$$\begin{aligned}\varepsilon = {} & \left[\frac{5}{2}R'T + \frac{R'\Theta}{e^{\Theta/T} - 1}\right](1 - m_D) + m_D R' T_D + \frac{3}{2}R'T(2m_D)(1 + m) \\ & + 2m_D R' \sum_i m_i T_i + \frac{E_c}{(n/3) - 1}\left[\left(\frac{\rho}{\rho^0}\right)^{n/3} - \frac{n}{3}\left(\frac{\rho}{\rho^0}\right)\right] \\ & + \frac{E_c}{(n/3) - 1}\left[\left(\frac{\rho}{\rho^0}\right)^{n/3} - \frac{n}{3}\left(\frac{\rho}{\rho^0}\right)\right] + E_c,\end{aligned} \tag{33}$$

where $m_k = 0.5[\tanh[7(T - 0.9T_K)] + \tanh[0.63]]$, $m = \sum_{i=1}^{5} m_i$, $R' = R/28.8$ is the gas constant for air, and, m_D ($0 \le m_D \le 1$; $T_D = 9.7$ eV), m_i ($0 \le m_i \le 1$; $T_{1\text{–}5} = 14.5, 29.6, 47.4, 77.5,$ and 97.5 eV), n (=9), ρ^0 (=1.113 g/cc), E_c (=2.52×10^9 ergs/g), and, Θ(= 3340 K), are the dissociation of molecular nitrogen, the ionization, intermolecular potentials, the maximum density of the air, the binding energy of fully compressed air, and the vibrational contributions in the energy equation, respectively.

A polynomial equation of state for water [22] is given by

$$p = (1 + \zeta)\left(\frac{G_1 + G_2 E + G_3 E^2 + G_4 E^3}{G_5 + G_6 E + G_7 E^2}\right) \quad \text{and} \quad G_i = \sum_{j=0}^{3} A_{ij}\zeta^3, \tag{34}$$

where p and E are expressed in terapascals, $\zeta = \rho/\rho^0 - 1$, $E = \varepsilon\rho^0$, and, $\rho^0 = 0.998$ Mg/m^3 (density at 298.5 K and standard pressure). The coefficients A_{ij} for these analytic expressions are presented in Table I. The range of applicability of Eq. (34) is $0.025 \le T \le 10$ eV and $0.998 \le \rho \le 40$ Mg/m^3, and $p \ge 10^{-2}$ MPa. In the numerical solution of present problem, the spatial scale to be resolved in the water will become progressively smaller as bubble collapse proceeds because the position of the interface decreases with time. If a fixed grid is adopted, an excessively large number of grid points are required. To avoid the problem, we introduced a moving grid during the bubble collapse period according to

$$z = \left(\frac{r}{a(t)}\right). \tag{35}$$

TABLE I
Numerical Values of Constants A_{ij}

i	A_{i0}	A_{i1}	A_{i2}	A_{i3}
1	0	2.190E−3	1.544E−1	2.160E−1
2	−1.340E−2	2.809E+1	1.990E+2	−1.114E+1
3	1.493E+3	3.016E+4	7.418E+3	3.184E+3
4	9.166E+4	7.468E+5	7.742E+4	4.722E+3
5	1.000E+0	6.723E+1	−6.347E+1	3.331E+1
6	1.625E+3	3.274E+4	−2.189E+3	−1.842E+3
7	1.931E+5	1.545E+6	8.734E+4	6.006E+3

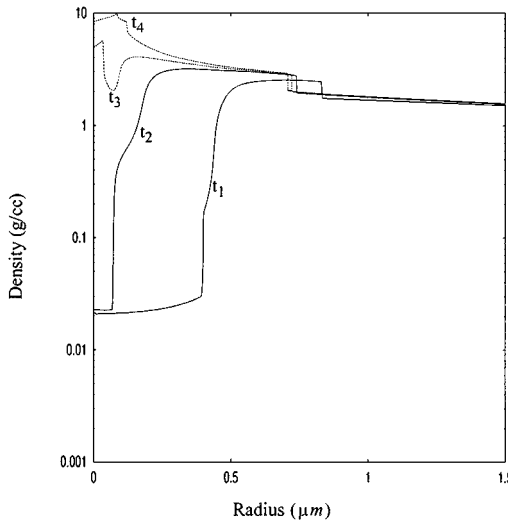

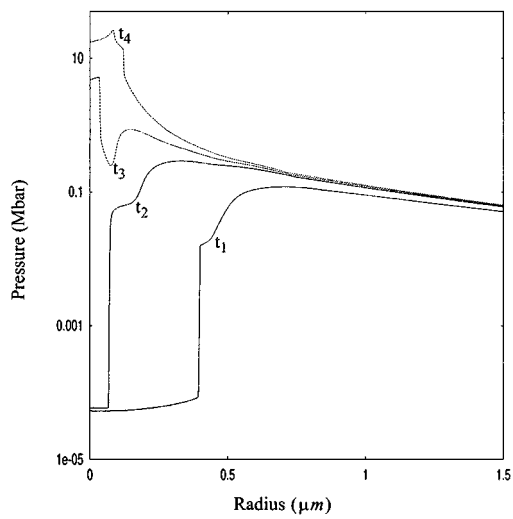

FIG. 10. The solutions for an imploding bubble with general equations of state for air and water; 600 cells inside the bubble and 2000 nonuniform mesh points in the water, with a moving grid.

For the bubble growth period, in terms of the original state variable, r, the sizes of the water zones are fixed. The bubble growth period had four equally sized air zones and 2000 water zones that increased geometrically in size from 0.3 μm at a_0, to 154 μm at R_F. Four air zones are enough for an accurate numerical evaluation because the interface velocity is much less than the sound speed in the gas during this period. At the end of the growth period ($a(t) = a_{\max}$), the complete solution was mapped onto the new mesh of 600 equally sized air zones, and the calculation proceeded. To find the solution on the moving grid, we used a mapping technique after integration of the Lagrangian step. Figure 10 shows spatial profiles of density and pressure at four times (t_{1-4}), where t_1 is the time at which the second shock has reached 0.4 μm. With t_1 taken as the reference time, t_{2-3} are $t_1 + 32$ ps, $t_1 + 42$ ps, and $t_1 + 52$ ps, respectively. This problem was previously considered by Moss *et al.* [21] using the Hydrocode, KDYNA [23, 24]. Their results and ours are nearly equivalent, except for the density profile near the geometric center after the reflection. The density profile near the center calculated with KDYNA is steeper than the present results using $B\text{-}Q\&H_L(0.25)$, due to the previously discussed artifacts associated with artificial viscosity.

5. CONCLUSION

Whenever a discontinuity appears in a solution, traditional numerical schemes based on central differencing, combined with artificial viscosity, are tremendously useful numerical techniques. However, with traditional artificial viscosity (Q) formulations, the Q-induced errors and the smearing of a shock make application of the methods unreliable. We have demonstrated that the new formulation presented herein provides good results without oscillations and Q-induced errors. Accurate answers and sharp shock capturing were obtained for Noh's shock wave problems (i.e., for plane geometry with uniform and nonuniform meshes and for spherical geometry), Sod's shock tube problem, and other shock problems for real equations of state. The superiority of the new method was confirmed using the Q-induced geometric error which was defined in this paper.

A summary of the advantages of the new algorithm are: (1) The present formulation of artificial viscosity (Q) is valid not only for a plane geometry but also for cylindrical and spherical geometries. (2) Since the present formulation is developed on the basis of a physical conservation of momentum correction, the additional amount of momentum introduced by Q is such that the geometric error is near zero. (3) The Q-heating error can be eliminated with the present filtered H formulation and the advantages described above are analogous for the present formulation of H. (4) A nonlinear numerical filter for eliminating nonphysical oscillations is simply implemented into the $Q\&H$ correction by intensifying the local correction terms in the equation up to their maximum values. This allows the use of a smaller Q coefficient. (5) The smearing of the shock by the new filtered $Q\&H$ formulation is small, so that the shocks are resolved within four mesh intervals, which is the maximum shock thickness using the present formulation. Similarly, a contact discontinuity is resolved within one mesh interval transition. Last, but not least, the new filtered $Q\&H$ formulation has proved to be a robust, accurate, and numerically efficient means of analyzing a wide range of one-dimensional problems which involve strong shock.

REFERENCES

1. J. von Neumann and R. D. Richtmyer, A method for the numerical calculation of hydrodynamic shocks, *J. Appl. Phys.* **21**, 232 (1950).

2. B. Engquist, P. Lötstedt, and B. Sjögreen, Nonlinear filters for efficient shock computation, *Math. Comp.* **5**, 509 (1989).
3. S. K. Godunov, A. V. Zabrodin, and G. P. Prokopov, A finite difference method for the numerical computation of discontinuous solutions of the equations of fluid dynamics, *Mat. Sb.* **47**, 357 (1959).
4. P. L. Roe, Approximate Riemann solvers, parameter vector, and difference schemes, *J. Comput. Phys.* **43**, 357 (1981).
5. L. C. Huang, Pseudo-unsteady difference schemes for discontinuous solutions of steady-state, one-dimensional fluid dynamics problems, *J. Comput. Phys.* **42**, 195 (1981).
6. A. Harten, High resolution schemes for hyperbolic conservation laws, *J. Comput. Phys.* **49**, 357 (1983).
7. S. Osher and F. Solomon, Upwind difference schemes for hyperbolic systems of conservation laws, *Math. Comp.* **38**, 339 (1981).
8. J. L. Steger and R. F. Warming, Flux vector splitting of the inviscid gasdynamic equations with application to finite-difference methods, *J. Comput. Phys.* **40**, 263 (1981).
9. J. Glimm, G. Marshall, and B. Plohr, A generalized Riemann problem for Quasi-one-dimensional gas flows, *Adv. in Appl. Math.* **5**, 1 (1984).
10. P. Colella, Glimm's method for gas dynamics, *SIAM J. Sci. Statist, Comput.* **3**, 76 (1982).
11. H. T. Huynh, Accurate upwind methods for Euler equations, *SIAM J. Numer. Anal.* **32**, No. 5, 2565 (1995).
12. R. Donat and A. Marquina, Capturing shock reflections: An improved flux formula, *J. Comput. Phys.* **125**, 42 (1996).
13. R. Menikoff, Errors when shock waves interact due to numerical shock width, *SIAM J. Sci. Statist. Comput.* **15**, No. 5, 1227 (1994).
14. W. F. Noh, Errors for calculations of strong shocks using an artificial viscosity and an artificial heat flux, *J. Comput. Phys.* **72**, 78 (1987).
15. D. J. Benson and S. Schoenfeld, A total variation diminishing shock viscosity, *Comput. Mech.* **11**, 107 (1993).
16. J. P. Morris and J. J. Monaghan, A switch to reduce SPH viscosity, *J. Comput. Phys.* **136**, 41 (1997).
17. P. Colella and P. R. Woodward, The piecewise parabolic method (PPM) for gas-dynamical simulations, *J. Comput. Phys.* **54**, 174 (1984).
18. C. A. J. Fletcher, *Computational Techniques for Fluid Dynamics* (Springer-Verlag, New York, 1988), Vol. 1, p. 278.
19. G. A. Sod, A survey of several finite difference methods for systems of nonlinear hyperbolic conservation laws, *J. Comput. Phys.* **27**, 1 (1978).
20. P. Glaister, An approximate linearised Riemann solver for the Euler equations for real gases, *J. Comput. Phys.* **74**, 382 (1988).
21. W. C. Moss, D. B. Clarke, J. W. White, and D. A. Young, Hydrodynamic simulations of bubble collapse and picosecond sonoluminescence, *Phys. Fluids* **6**, 2979 (1994).
22. F. H. Lee, *Equation of State of Water*, LLNL Report, UCRL-52190 (1976).
23. J. O. Hallquist, *DYNA2D—An Explicit Finite Element and Finite Difference Code for Axisymmetric and Plane Strain Calculations (User's Guide)*, LLNL Report, UCRL-52429 (1978).
24. J. L. Levatin, A. V. Attia, and J. O. Hallquist, *KDYNA User's Manual*, LLNL Report, UCRL-ID-106104 (1990).